Nandagiri, VK.; Gentile, P.; Chiono, V.; Tonda-Turo, C.; Matsiko, A.; Ramtoola, Z.; Montevecchi, FM.... (2011). Incorporation of PLGA nanoparticles into porous chitosan-gelatin scaffolds: Influence on the physical properties and cell behavior. Journal of the Mechanical Behavior of Biomedical Materials. 4(7):1318-1327. https://doi.org/10.1016/j.jmbbm.2011.04.019

Incorporation of PLGA nanoparticles into porous chitosan–gelatin scaffolds: Influence on the physical properties and cell behavior

Vijay Kumar Nandagiri [a,b,c], Piergiorgio Gentile [a], Valeria Chiono [a], Chiara Tonda-Turo [a], Amos Matsiko [c], Zeibun Ramtoola [b], Franco Maria Montevecchi [a], Gianluca Ciardelli [a]

[a]Department of Mechanics, Politecnico di Torino, Corso Duca degli Abruzzi 24, 10129 Turin, Italy

[b]School of Pharmacy, Royal College of Surgeons in Ireland, 123, St. Stephen Green, Dublin 2, Ireland

[c]Department of Anatomy, Royal College of Surgeons in Ireland, 123, St. Stephen Green, Dublin 2, Ireland

∗ *Corresponding author at:* Department of Mechanics, Politecnico di Torino, Corso Duca degli Abruzzi 24, 10129 Turin, Italy. Tel.: +39 011 5646969; fax: +39 011 5646999.

E-mail address: vijay.polito@gmail.com (V.K. Nandagiri).

Abstract

Bone regeneration can be accelerated by localized delivery of appropriate growth factors/biomolecules. Localized delivery can be achieved by a 2-level system: (i) incorporation of biomolecules within biodegradable particulate carriers (nanoparticles), and (ii) inclusion of such particulate carriers (nanoparticles) into suitable porous scaffolds. In this study, freeze-dried porous chitosan–gelatin scaffolds (CH–G: 1:2 ratio by weight) were embedded with various amounts of poly(lactide-co-glycolide) (PLGA) nanoparticles, precisely 16.6%, 33.3% and 66.6% (respect to CH–G weight). Scaffolds loaded with PLGA nanoparticles were subjected to physico-mechanical and biological characterizations including morphological analysis, swelling and dissolution tests, mechanical compression tests and cell viability tests. Results showed that incorporation of PLGA

nanoparticles into porous crosslinked CH–G scaffolds: (i) changed the micro-architecture of the scaffolds in terms of mean pore diameter and pore size distribution, (ii) reduced the dissolution degree of the scaffolds, and (iii) increased the compressive modulus. On the other hand, the water uptake behavior of CH–G scaffolds containing PLGA nanoparticles significantly decreased. The incorporation of PLGA nanoparticles did not affect the biocompatibility of CH–G scaffolds.

Keywords: Chitosan; Gelatin; Genipin; Poly(lactide-co-glycolide); Porous scaffolds; Nanoparticles

1. Introduction

Bone regeneration is a complex cascade of biological events controlled by numerous bioactive molecules that provide signals at local injury sites allowing progenitors and inflammatory cells to migrate and trigger healing processes. Conventional tissue engineering strategies utilize combination of cells, biodegradable scaffolds and systemic administration of bioactive molecules to promote natural processes of tissue regeneration and development (Borenstein et al., 2007). However, systemic administration of biomolecules such as growth factors often produces poor results, probably due to their short biological half-life, lack of tissue specificity, long term instability, and potential dose dependent carcinogenicity (Kobsa and Saltzman, 2008, Lee and Shin, 2007). In addition to this, a well timed and localized delivery of biomolecules from the scaffold is necessary to achieve the desired biomimetic effect (Vasita and Katti, 2006, Zisch et al., 2003).

A number of strategies for controlled biomolecule delivery from scaffolds has been developed for bone tissue engineering. One of the most common methods to achieve controlled and localized release of biomolecules is to incorporate them within biomaterials during the phase of scaffold fabrication. According to this approach, the properties of the scaffolds, such as pore size and crosslinking density, control the biomolecule release rate by diffusion. In addition, the rate of

scaffold degradation affects the biomolecule release rate over a prolonged time period (Tachibana et al., 2006, Kim et al., 2003, Bonadio et al., 1999). Such approaches are often unsatisfactory, as the cells may be exposed initially to an excessive concentration of biological molecules which could result toxic and, subsequently, to ineffective concentration levels of the biomolecules as a consequence of their short half life and clearance. To overcome these problems, researchers have encapsulated biomolecule(s) into polymeric micro/nanoparticulate systems, to be subsequently incorporated into scaffolds for localized and/or controlled delivery of the biomolecule(s). These micro/nanoparticulate carrier systems allow controlled release of incorporated biomolecule(s) over time and, in addition, increase the biological half life of the biomolecule(s), as they protect them from degradation/clearance. Furthermore, the release kinetics of the target biomolecules can be modulated by changing the composition of the particulate carrier system, the amount of drug encapsulated and the size of the micro/nanoparticles.

However, when micro/nanoparticles are incorporated into prefabricated porous scaffolds, they often tend to aggregate, which may not serve the purpose of controlled/spatial delivery of biomolecules (Langer, 1998, Jeong et al., 1997, Ma, 2008). One approach to overcome these limitations is to suspend the biomolecules-loaded micro/nanoparticles into biomaterial solutions during the crosslinking phase of scaffold fabrication. Few studies in literature have reported the incorporation of micro-scale particulate carrier systems within porous scaffolds for localized delivery of biomolecules. For example, Perets et al. incorporated bFGF-loaded PLGA microparticles into alginate porous scaffolds to enhance vascularization after implantation in rat peritoneum. They reported a fourfold increase in number of penetrating capillaries into the bFGF releasing scaffolds as compared to their control counterparts (Perets et al., 2003). Furthermore, Khil et al. have designed a type of porous chitosan scaffold, containing chitosan microspheres

loaded with TGF-β1, to enhance chondrogenesis (Khil et al., 2003). They demonstrated that the scaffolds containing the loaded chitosan microspheres significantly increased the cell proliferation and production of ECM. A similar approach using chitosan-based materials has been reported by Lee et al. (2004), where three-dimensional collagen/chitosan/glycosaminoglycan scaffolds were seeded with rabbit chondrocytes and combined with TGF- β1-loaded chitosan microspheres. This set-up allowed for evaluating the effect of released TGF- β1 on the chondrogenic potential of rabbit chondrocytes in such combined systems.

In all these studies, the authors have mainly emphasized the possibility to achieve a desired biological response by localized delivery of biomolecules. However, the influence of particle incorporation on the physico-mechanical properties of porous scaffolds has not been properly assessed. Recently, Banarjee et al. have reported the effect of poly(lactide-co-glycolide) (PLGA) microsphere incorporation on the physical properties as well as the cellular performance of the freeze-dried gelatin scaffolds (Banerjee et al., 2009). However, these effects may differ when blends of two or more polymers are used to fabricate porous scaffolds and these effects are largely dependent on the size of incorporated particles. Nano/submicron particles offer numerous advantages over microparticles such as more homogeneous distribution of particles within the polymeric solution during the crosslinking step of scaffold fabrication and availability of more particles for same equivalent weight of carriers. Moreover, the lengthy diffusion times of biomolecules from microparticle(s) carrier matrix can be avoided when nano/submicron particles are used, which could facilitate the pulsed release of incorporated biomolecules. A further advantage with nano/submicron particles over microparticles is the prevention of acidic microenvironment within particle matrix, which is a consequence of hydrolytic degradation of PLGA into lactic and glycolic acids.

In this study, PLGA nanoparticles, containing a model protein, bovine serum albumin (BSA), were incorporated into freeze-dried porous scaffolds based on a chitosan–gelatin blend (CH–G) crosslinked with genipin (GP). Such a system primarily acts as a local regulator to control doses and kinetics of released growth factor, thus increasing their potential retention time at therapeutic concentration levels (Kobsa and Saltzman, 2008, Silvia et al., 2007).

CH was selected as it is a biodegradable, biocompatible and nontoxic naturally derived polysaccharide which exhibits hemostatic, antimicrobial and gel-forming properties (Madihally and Matthew, 1999). Scaffolds based on CH have been reported to display hydrophilic and cell adhesive/differentiating characteristics (VandeVord et al., 2002, Suh and Matthew, 2000). Furthermore, the inherent osteoconductive nature of CH enhances its potential for bone tissue engineering applications (Lahiji et al., 2000). G is a protein derived from collagen, and it has been frequently applied in artificial skin, bone grafts, and scaffolds for tissue engineering (Esposito et al., 1996, Kawai et al., 2000, Zhao et al., 2002, Ito et al., 2003, Chang et al., 2003). Its wide use in the biomedical field is motivated by the presence of Arg-Gly-Asp (RGD)-like sequences that promote cell adhesion and migration (Shen et al., 2000).

When CH and G are blended together, the spatial arrangement of G integrin ligands and CH polycationic groups interacting with the anionic cell surface is affected. Thus, blending influences cell adhesion, cellular bioactivity and tissue remodeling process and ultimately the quality of the regenerated tissue (Huang et al., 2005). The mechanical properties and water stability of CH–G blend can be increased by crosslinking with suitable noncytotoxic crosslinking agents. In this work, genipin, an aglycone derived from geniposide which is extracted from the fruit of Gardenia Jasminoides Ellis, was selected as a crosslinker for CH–G blend (Mi, 2005). PLGA nanoparticles

were selected as they have a recognized biocompatibility and efficiency in the delivery of growth factors, proteins or drugs, in a time dependent manner, both in vitro and in vivo (Muthu, 2009).

Freeze-drying is one of the most applied methods for fabrication of scaffolds based on CH–G blends. Freeze-drying method involves the formation of inter/intraconnected ice crystals inside the polymer solution(s) during the freezing stage, which then form pores during sublimation leading to a porous three-dimensional polymeric scaffold (Huang et al., 2005).

The introduction of hydrophobic particulate carriers to obtain a localized delivery of bioactive molecules may change the pattern of ice crystal formation and distribution during freezing, which in turn may influence the scaffold micro-architecture.

In this work, the effect of PLGA nanoparticles incorporation on the physical and biological properties of freeze-dried GP-crosslinked CH–G scaffold(s) were investigated by analyzing the scaffold micro-architecture, porosity, swelling degree, mechanical compressive strength, in vitro dissolution, cell attachment and cell viability using clonal human osteoblast cell line (hFOB). HFOB cell line is a clonal, conditionally immortalized human fetal cell line capable of osteoblastic differentiation and bone formation, that provides a homogeneous, rapidly proliferating model system for studying human osteoblast differentiation, physiology, and effects of cytokines on osteoblasts (Harris et al., 1995). HFOB is a widely used cell line to reflect human bone biology; hence, this cell line was selected to analyze cell viability into CH–G scaffolds incorporating PLGA nanoparticles.

2. Materials and methods

Chitosan (CH), gelatin (G), fraction V bovine serum albumin (BSA), poly vinyl alcohol (MW: 30–70 kDa, >87%–90% hydrolyzed) (PVA) and trehalose were purchased from Sigma Chemicals Co.

Poly(DL-lactide-co-glycolide) (PLGA) 50:50 (RG 504 H, MW 48,300 Da) was obtained from Boehringer Ingelheim Pharma GmbH & Co. KG, (Ingelheim, Germany). Genipin (GP) was acquired from Challenge Bioproducts Co., Taiwan. For cell culture studies, hFOB (ATCC, MA) pre-osteoblastic cells cultured under standard conditions (5% CO2, 37 °C) were used. Other reagents for culture medium include Hams F12 and Dulbecco's modified Eagle's medium (without phenol red) (Gibco, UK), 10% fetal bovine serum (Sigma-Aldrich), 1% penicillin/streptomycin 10 mg/ml (Sigma-Aldrich), trypsin–EDTA (Sigma-Aldrich). Alamar blue dye was obtained from Bioscience, Ireland. All reagents and solvents used were HPLC grade or analytical grade.

2.1. Preparation of CH–G scaffolds

CH and G were dissolved in 0.5 M acetic acid (Sigma, Italy) at CH–G 1:2 weight ratio obtaining a solution with 3% (w/v) concentration by stirring for 12 h at 40 °C. GP crosslinker was added to the solution at defined weight percentage (2.5% wt/wt with respect to the CH–G amount). The mixture was kept at 50 °C under stirring until a gel started to form (approximately 30 min). The gel was spread on Petri dishes, pre-freezed at −20 °C for 12 h and freeze-dried (Scanvac, CoolSafe) for 24 h to obtain porous CH–G matrices. After freeze-drying, samples were washed in 70%, 90% and 100% w% ethanol, for 20 min to neutralize the acid content and then repeatedly washed in de-mineralized water till pH of washing medium was 7. Washing was also performed to remove un-reacted GP residues (Chiono et al., 2008).

2.2. Preparation of BSA-loaded PLGA nanoparticles

PLGA nanoparticles were prepared using a modified double emulsion–solvent diffusion method (Cohen-Sela et al., 2009). The procedure in brief is as follows. One ml of BSA aqueous phase, containing 3% (w/v) trehalose in PBS, was added to 4 ml of 25 mg/ml PLGA solution in ethyl

160 acetate and subjected to probe sonication (Branson sonifier 150, Branson Ultrasonics Corporation
161 41 Eagle Road, Danbury, CT) for 2 min at level 3. The resulting emulsion was transferred into 4
162 ml of 2.5% (w/v) PVA (pH 4.5) solution and sonicated for 2 min at level 3. After 2 min of
163 sonication, the mixture was transferred into 25 ml of 1% (w/v) PVA solution and homogenized for
164 3 min at a speed of 13,500 rpm to form a double emulsion. The organic solvent was evaporated by
165 stirring the double emulsion with 25 ml of normal saline at 30 °C for 3–4 h (until the solvent was
166 evaporated). The nanoparticles were collected by ultracentrifugation at 30,000 rpm for 30 min
167 (Ultracentrifuge Sorvall RC 5C plus, Maryland, USA), washed three times with purified water and
168 freeze-dried (Freezone 6, Labconco, MO: −57 °C, 0.03 mbar, 24 h).

169 Blank nanoparticles were prepared similarly to the above procedure except for the inclusion of
170 BSA in internal aqueous phase.

171 **2.3. Characterization of nanoparticles**

172 Lyophilized nanoparticles were characterized for particle size, zeta potential, moisture content and
173 surface morphology. For measuring particle size and zeta potential, freeze-dried PLGA
174 nanoparticles were dispersed in deionized water (1 mg/ml). Approximately 0.1 ml of this
175 suspension was diluted in filtered deionized water and transferred in a folded capillary cell avoiding
176 the formation of any air bubbles. The mean particle diameter and polydispersity index of particles
177 was determined using non-invasive back scatter (NIBS) technology, which allows sample
178 measurement in the range of 0.6–6000 nm by means of photon correlation spectroscopy using a
179 Zetasizer (Nano ZS/ZEN 3600, Malvern Instruments, UK). The measurement was carried out using
180 a 4 mW He–Ne laser as a light source at a fixed angle of 173°. The following parameters were used
181 for the measurements: 1.339 medium refractive index, 0.88 mPa.s medium viscosity, and 78.54

182 dielectric constant, 25 °C temperature. Size measurements were carried out by at least 5 runs and
183 in triplicate for each sample and results were expressed as the mean size ± standard deviation (SD).

184 The morphology of PLGA nanoparticles was analyzed by scanning electron microscopy (SEM).
185 Freeze-dried PLGA nanoparticles were fixed onto metallic studs with double-sided conductive tape
186 (diameter 12 mm, Oxon, Oxford instruments, UK) and coated with gold for 4 min under nitrogen
187 atmosphere in a Blazers of a sputter coating unit (Agar Sputter coater, Agar Scientific Ltd., Essex,
188 UK). A LEO 1450 VP (Leo Electron microscopy Ltd., Cambridge, UK) scanning electron
189 microscope (SEM) was used with an acceleration voltage of 1.00 kV and a secondary detector
190 (Holzer et al., 2009).

191 **2.4. Preparation of PLGA nanoparticles-embedded CH–G scaffolds**

192 PLGA nanoparticles-embedded CH–G scaffolds were obtained by dispersing an aqueous
193 suspension of PLGA nanoparticles into CH–G blend solution (3% w/v) at different concentrations:
194 5 mg, 10 mg and 20 mg per ml of CH–G blend solution, respectively (16.6; 33.3; 66.6 w/w PLGA
195 loading with respect to CH–G weight). CH–G scaffolds without nanoparticles were prepared for
196 use as a control for experimental tests. The ensuing preparative stages, such as crosslinking,
197 lyophilization, and neutralization were performed using the same protocols as described in
198 paragraph 2.1.

199 **2.5. Study of scaffold micro-architecture**

200 Pore size analysis of the scaffolds was carried out using a technique previously described by
201 O'Brien et al. (2004).

202 A total of three scaffolds per group were used in this analysis. Three fixed scaffold sections were
203 analyzed: top, middle and bottom surface. In detail, samples were first embedded in JB-4-

glycolmethacrylate (Polysciences Europe, Eppelheim, Germany). The embedded samples were sectioned into 10 μm thick slices using a microtome (Leica RM 2255, Leica, Germany) and the 20th slice (representative of the section located at 200 μm distance from the surface) was used as the middle section. Four serial sections were obtained from each fixed location of each scaffold to obtain a total of 12 serial sections. The sections were then mounted on glass slides and stained with toluidine blue, then observed under a microscope (Eclipse 90i, Nikon, Japan). Digital images were then taken at 10X magnification (image quality 1280×1024–16 bit, exposure time 3 ms) using a digital camera (DS Ri1, Nikon, Japan). A total of 36 images of serial sections from each scaffold group were obtained. The digital images were evaluated using a specifically developed MatLab (The MathWorks Inc., MA, USA) pore topology analyzer software. In order to yield correct results, the software was calibrated by setting the pixel to micron ratio using the scale bar on the images. The software successively transformed the original images into binary images, removed unwanted blotches and generated the pore size. The pore size was defined as the diameter of a circle with a cross-sectional area equivalent to that of the best fit ellipse generated by the software (at least 50 pores/section were considered for each analysis). The mean pore size was calculated from the images of each scaffold group statistical significance of data between the groups was evaluated.

2.6. Scaffold morphology

Scaffold morphology was analyzed using SEM (LEO 1450 VP; Leo Electron microscopy Ltd., Cambridge, UK) to study the influence of PLGA nanoparticles into scaffold micro-architecture. Three samples were obtained by fracturing each scaffold type and the fractured sections of these samples were analyzed by SEM. Prior to observation through SEM, scaffolds were sputter coated with gold and analyzed at an accelerating voltage of 20 kV.

2.7. Study of the water uptake ability (swelling test)

The effect of nanoparticle incorporation on water absorption capacity of the scaffolds was determined after immersion of cylindrical scaffolds with 8 mm diameter and approximately 4 mm thickness in 3 ml of PBS (100 mM, pH 7.4) at 37 °C. Wet weight was determined after 24 h of incubation. The percentage of water absorption (W_{sw}) of the scaffolds was calculated from the expression (Banerjee et al., 2009, Thein-Han et al., 2009):

$$W_{\mathrm{sw}} = \left[\left(W_{24\mathrm{h}} - W_0\right)/W_0\right] \times 100 \quad (1)$$

where, W_{24} represents the wet weight of scaffolds after 24 h of incubation and W_0 is the initial weight of the scaffolds. The values were expressed as mean ± SD (n=3).

2.8. Mechanical tests

Uniaxial compressive tests were carried out on cylindrical scaffolds with 8 mm diameter and 4 mm height. Samples were pre-hydrated in PBS (100 mM, pH 7.4) for 1 h. All tests were carried out in a bath of PBS (100 mM, pH 7.4) at room temperature, using a mechanical testing machine (Zwick-Roell, Germany) fitted with a 5 N load cell. The tests were carried out on unconfined and unlubricated platens. The cross-head speed was set at 0.007mm s^{-1} and the load was applied until the specimen was compressed at approximately 10% of its original length. The tests were conducted at a strain rate of 10% per minute. Each sample was tested in triplicate and the stress was calculated by dividing the applied force with the initial scaffold surface area, whereas strain was calculated from the displacement of the scaffolds in relation to the original thickness. A Matlab program was run to obtain the stress–strain curves from the acquired data. The compressive modulus (E) was calculated as the slope of a linear fit to the stress–strain curves over 2%–5% strain (Al-Munajjed and O'Brien, 2009). Data on the compressive modulus were averaged on three samples for each scaffold type.

2.9. Dissolution study

To study the effect of nanoparticle loading on in vitro dissolution of scaffolds, cylindrical scaffold samples of 8 mm diameter and approximately 4 mm thickness were incubated in 3 ml of PBS (pH 7.4) for 10 days at 37 °C. The dissolution degree was calculated in terms of percentage weight loss ($\%W_L$) using the formula (Banerjee et al., 2009):

$$\%W_L = [(W_{10} - W_0)/W_0] \times 100 \quad (2)$$

where, W_{10} is the dry weight of scaffolds after 10 days of incubation in PBS and W_0 is the initial weight. The values were expressed as the mean ± SD ($n=3$).

2.10. Cell culturing and seeding on scaffolds

HFOB (ATCC, MA) pre-osteoblastic cells were cultured under standard conditions (5% CO2, 37 °C). Cells were routinely grown to 80% confluency in T175 culture flasks (Sarstedt, Ireland) containing culture media; a 1:1 ratio of Hams F12 and Dulbecco's modified Eagle's medium (without phenol red), 10% fetal bovine serum, 1% penicillin/streptomycin (Sigma-Aldrich). Expanded hFOB cells of passage 5 were harvested with trypsin–EDTA treatment, centrifuged and resuspended in the culture medium. Aliquots of cell suspensions were then evenly seeded by instillation onto three samples of each scaffold type for each time interval to be analyzed to form cell-seeded scaffold constructs with a final seeding density of 4×106 cells (2×106 cells/each side of scaffold). The constructs were then placed in sterile 6 well plates and 5 ml of the growth medium were added into each well after 4 h incubation of cells to allow their attachment. During the culture period, the medium was exchanged every two days time interval. Scaffolds were incubated up to 11 days in the culture medium.

2.11. Cell attachment and viability of hFOB cells on CH–G scaffold

At fixed time intervals (1 day, 2 days, 5 days, and 11 days), metabolic viability of hFOB cells on the scaffolds was determined by replacing media surrounding the cell-seeded constructs with that containing 10% v/v Alamar blue dye (Bioscience). The samples

were incubated in an orbital shaker at 37 °C, at a shaking rate of 50 rpm for 4 h. After 4 h, 100

l of media were transferred into a 96 well microplate and their UV–visible absorbance at 570 and 610 nm was measured using a spectrophotometer. Samples were measured in triplicate for each scaffold type.

After collecting samples for Alamar blue assay, all scaffolds were washed three times by immersing in sterile PBS and then incubated in fresh 5 ml growth medium. The percentage of reduced dye as a function of cell viability was calculated in accordance with manufacturer's recommendations (Keogh et al., 2010).

2.12. Statistical analysis

Experiments were run in triplicate for each sample. All data were expressed as mean ± SD for n=3. Statistical analysis was determined by using Analyse-it v2.22 software. The statistical differences between groups were calculated using Kruskal–Wallis One Way Analysis of Variance on Ranks (ANOVA). Statistical significance was declared at $p < 0.05$

3. Results

3.1. Characterization of PLGA nanoparticles

The PLGA nanoparticles prepared by double emulsion–solvent evaporation method showed a mean diameter of 205.0 ± 3.9 nm, with a polydispersity index of 0.23 ± 0.04 (*n=3*) (Fig. 1(a)–(b)). SEM images of the nanoparticles showed their regular spherical shape, smooth surface and the absence

of aggregation. Moreover, no differences were observed in the morphological properties of nanoparticles due to the incorporation of BSA protein (Fig. 1(b)).

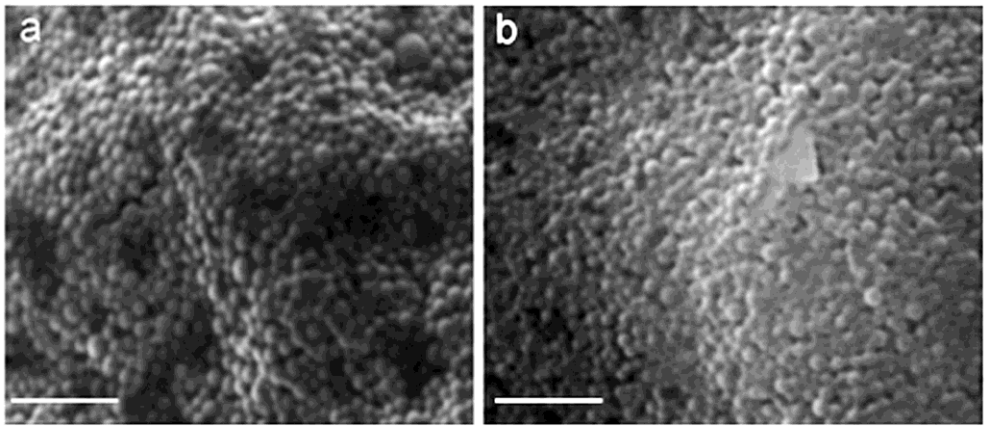

Fig. 1. SEM images of (a) unloaded PLGA and (b) BSA-loaded PLGA nanoparticles (bar: 1 μm).

3.2. Scaffold morphology

SEM micrographs of PLGA nanoparticles-embedded CH–G scaffolds (Fig. 2(a)–(c)) showed that PLGA nanoparticles were uniformly distributed on the pore walls independently on the amount of PLGA nanoparticles incorporated. However, some aggregates of PLGA nanoparticles were observed as the amount of particles increased (Fig. 2(c)).

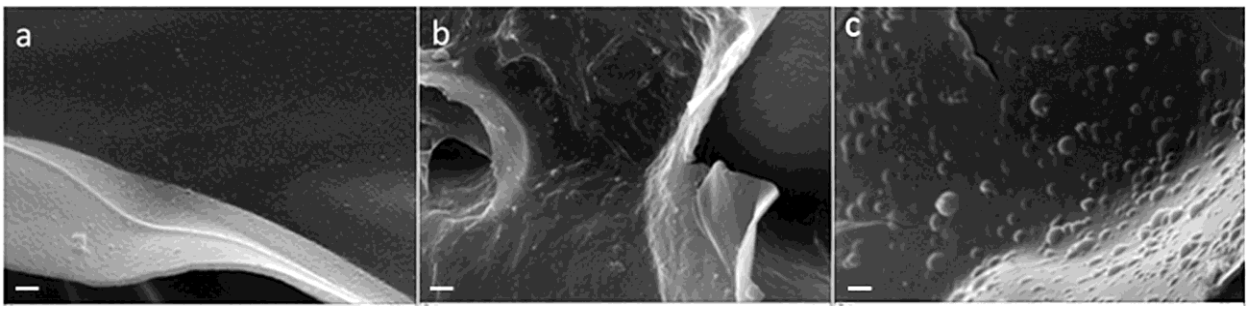

Fig. 2. SEM images of fractured sections of CH–G scaffolds showing distribution of PLGA nanoparticles on pore walls of CH–G scaffolds doped with: (a) 16.6% w/w, (b) 33.3% w/w and (c) 66.6% w/w of PLGA nanoparticles (bar: 2 μm).

306 Incorporation of PLGA nanoparticles into freeze-dried CH–G scaffolds did not affect significantly
307 the micro-architecture of scaffolds: all scaffold types showed a porous structure with pore
308 interconnection (Fig. 3(a)–(d)).

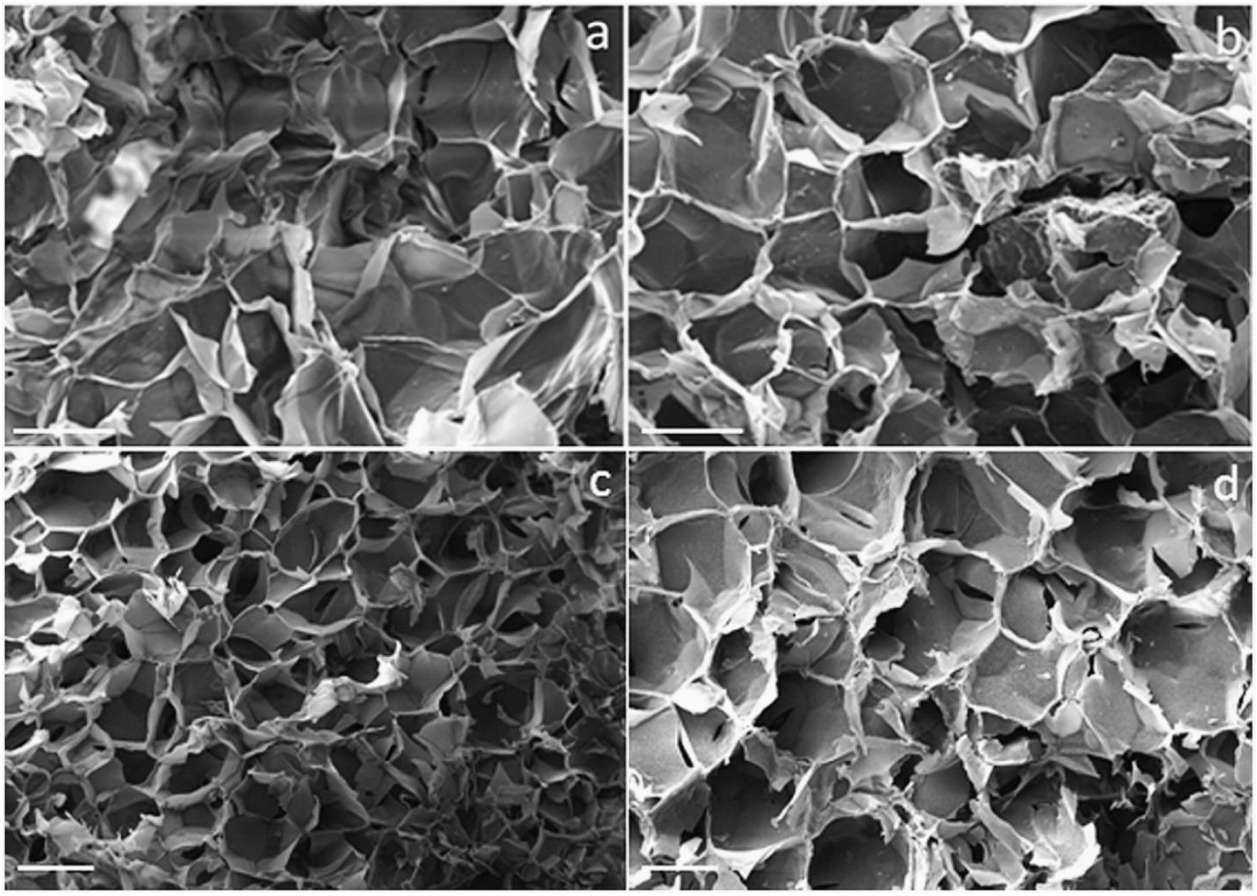

309

310 Fig. 3. SEM images of fractured sections of CH–G scaffolds embedding different amounts of
311 PLGA nanoparticles: (a) 0% w/w (control), (b) 16.6% w/w, (c) 33.3% w/w, and (d) 66.6% w/w of
312 PLGA nanoparticles (bar 200 μm).

313

314 Fig. 4 shows the mean pore size calculated according to the method described at paragraph 2.5.
315 Incorporation of PLGA nanoparticles into CH–G scaffolds did not change significantly the mean
316 pore size for the scaffolds loaded with 16.6% and 33.3% w/w nanoparticles (110±40 μm at 16.6%

(w/w) loading and 146±63 μm at 33.3% (w/w) loading) as compared to the control scaffolds (mean pore size of 130±37 μm). On the other hand, an increase in the mean pore size (194±70 μm) was observed when 66.6% (w/w) PLGA nanoparticles were incorporated.

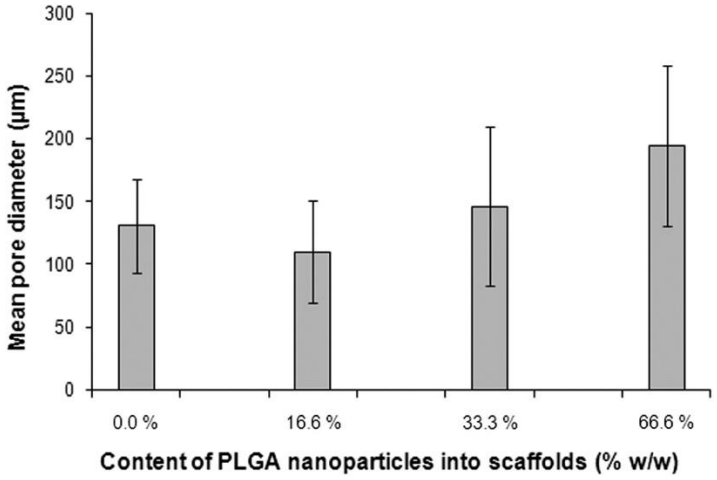

Fig. 4. Mean pore diameter of CH–G scaffolds as a function of PLGA nanoparticle amount. For each scaffold type, 50 pores were analyzed to get the mean pore size. Values are mean ± SD (*n=3*).

The mean pore size distribution of the PLGA nanoparticles-embedded CH–G scaffolds is shown in Fig. 5. In the case of control CH–G scaffolds, around 60% of pores were in the 100–150 μm size range, around 5% of pores had a size lower than 75 μm or higher than 200 μm and 15% of pores were in the 75–100 μm or 150–200 μm size ranges.

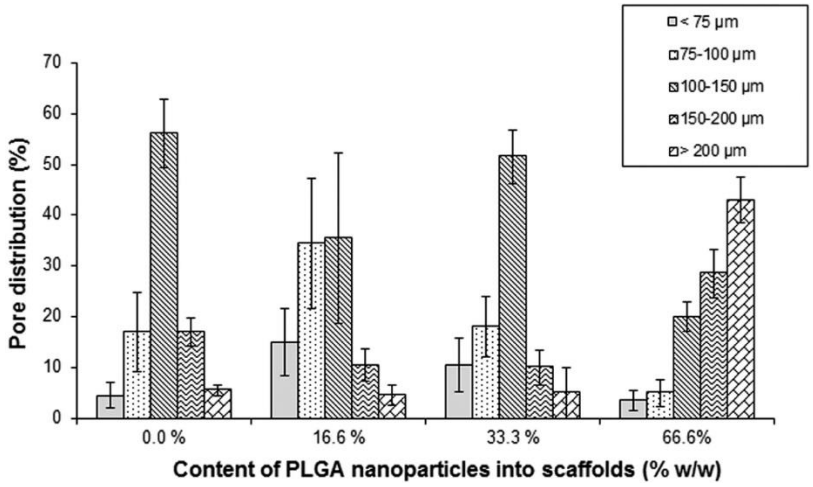

Fig. 5. Effect of the amount of nanoparticles on pore size distribution. At least, 50 pores were analyzed to get the mean pore size distribution. Values are mean ± SD (*n=3*).

The incorporation of 16.6% (w/w) PLGA nanoparticles resulted in 15% of pores with a size lower than 75 μm, 5% of pores with a size above 200 μm, 35% of pores in 75–100 μm size range, 35% in the 100–150 μm size range and the remaining 10% in 150–200 μm size range.

The incorporation of 33.3% (w/w) PLGA nanoparticles resulted in 52% of pores in the 100–150 μm size range, 10% in 150–200 μm size range, 18% in 75–100 μm size range and the remaining 10% were with a lower size than 75 μm.

Finally, the incorporation of 66.6% (w/w) of PLGA nanoparticles resulted in larger pores: around 45% of pores showed a higher size than 200 μm, 30% were in 150–200 μm size range and the remaining 25% showed a lower size than 150 μm.

In conclusion, pore size distribution of the control scaffolds and CH–G scaffolds incorporating 16.6% and 33.3% (w/w) PLGA nanoparticles was only slightly different with no change in the overall mean pore size (as shown in Fig. 4). On the other hand, in the case of CH–G scaffolds incorporating 66.6% (w/w) PLGA nanoparticles, pore size distribution was significantly changed as compared to the control scaffold and scaffolds containing 16.6% and 33.3% (w/w) nanoparticles, with a prevalence of pores having size higher than 150 μm. For this reason, the measured mean pore size of scaffolds with 66.6% (w/w) PLGA nanoparticles was larger than the values measured for the other samples (Fig. 4).

3.3. Swelling behavior

The water uptake ability of the control scaffolds after 24 h of incubation in PBS was 1245 ± 56% (Fig. 6). As expected, the incorporation of hydrophobic PLGA nanoparticles reduced the water

uptake, which was approximately similar for loading values of 16.6% (w/w) (524 ± 35%) and 33.3% (w/w) (631±190%) (Fig. 6). Scaffolds loaded with 66.6% (w/w) PLGA nanoparticles displayed the lowest swelling degree (352 ± 17%).

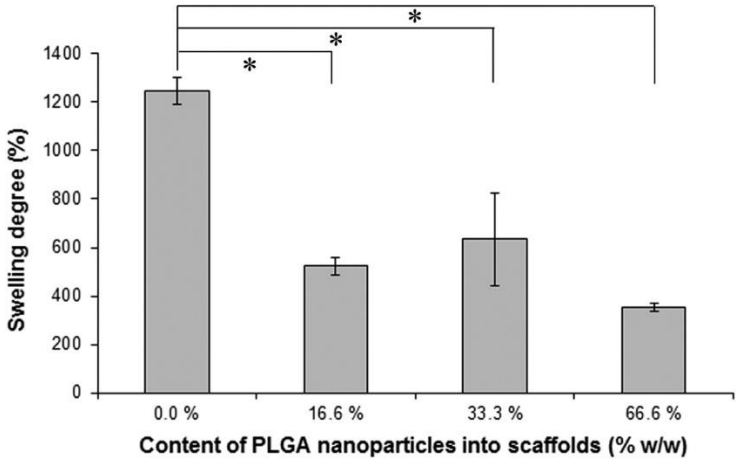

Fig. 6. Effect of PLGA nanoparticles incorporation on water uptake of scaffolds after 24 h of incubation in PBS. Columns are the mean values; bars represent the standard deviation (*n=3*). Data show statistical difference with respect to the control * ($p < 0.05$).

In conclusion, the introduction of a relatively small amount of PLGA nanoparticles greatly reduced the swelling degree as compared to control CH–G scaffolds: the homogeneous distribution of hydrophobic PLGA nanoparticles into the CH–G walls significantly decreased the water uptake.

3.4. Mechanical properties of scaffolds

The mechanical compressive strength of the porous CH–G scaffolds was measured by calculating the compressive modulus from stress–strain data obtained under a compressive load at a constant speed in wet conditions. The compressive modulus of CH–G scaffolds embedding PLGA nanoparticles is reported in Fig. 7. Among the tested samples, control scaffolds displayed the minimum compressive modulus (6.4 ± 0.8 kPa). For scaffolds containing 33.3% (w/w) PLGA

nanoparticles, the compressive modulus (54.3 ± 1.9 kPa) was increased approximately by 9 times in comparison to that of the control scaffolds.

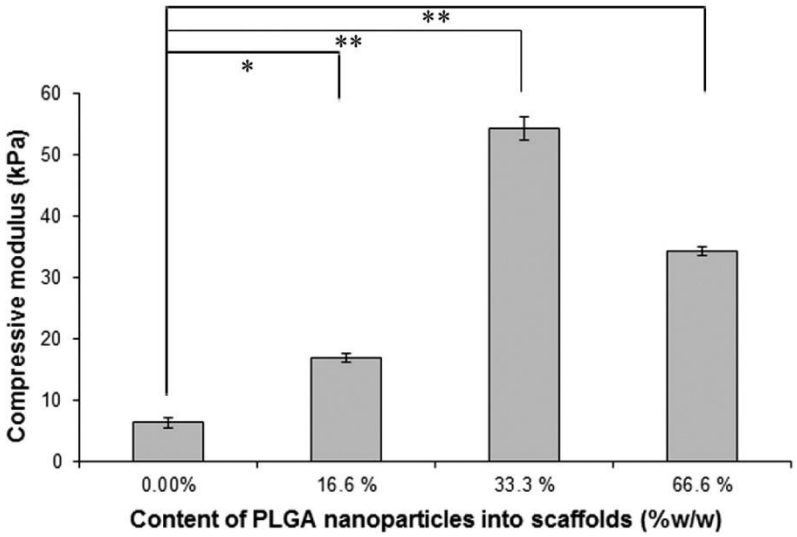

Fig. 7. Compressive modulus of CH–G scaffolds as a function of nanoparticle amount. Columns are the mean values; bars represent standard deviation ($n=3$). Data show statistical difference with respect to the control * ($p < 0.05$) and ** ($p < 0.0001$).

The compressive modulus of scaffolds containing 16.6% (w/w) and 66.6% (w/w) PLGA nanoparticles was increased approximately by three and six times as compared to that of the control scaffolds with the values of 16.9 ± 0.6 kPa and 34.3 ± 0.7 kPa, respectively.

In conclusion, the addition of PLGA nanoparticles significantly increased the compressive modulus of CH–G scaffolds. However, in case of scaffolds with highest amount of nanoparticles (66.6% (w/w)), the compressive modulus was decreased as compared to that of scaffolds containing 33.3% (w/w) of nanoparticles.

3.5. Dissolution tests

Fig. 8 shows the dissolution degree of CH–G scaffolds after 10 days incubation in PBS as a function of the amount of incorporated PLGA nanoparticles. The incorporation of 16.6% and 33.3% (w/w) PLGA nanoparticles had no significant effect on the dissolution degree of CH–G scaffolds. On the other hand, scaffolds containing 66.6% (w/w) PLGA nanoparticles showed an increased dissolution degree. The different behavior of the CH–G scaffolds containing 66.6% (w/w) PLGA nanoparticles could be a consequence of their higher porosity and mean pore size as compared to the CH–G control scaffolds, increasing the dissolution rate.

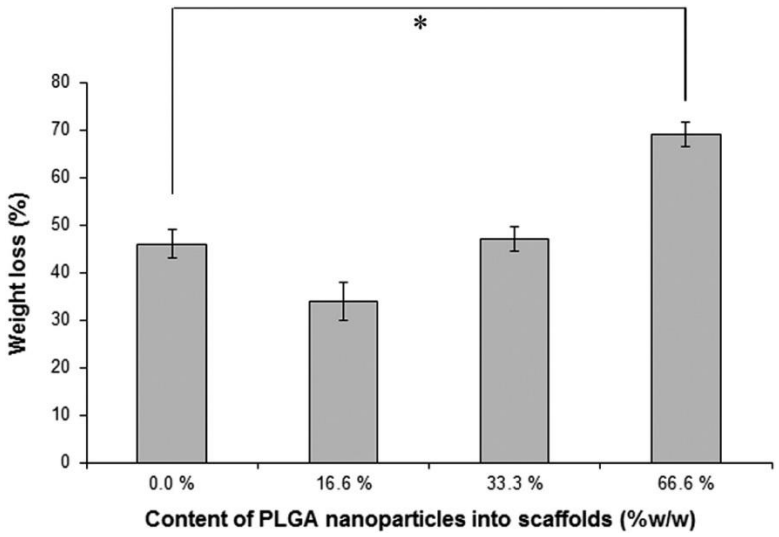

Fig. 8. Effect of amount of PLGA nanoparticles incorporation on dissolution properties of scaffolds after 10 days of incubation in PBS. Columns are the mean values; bars represent standard deviation ($n=3$). Data show statistical difference with respect to the control * ($p < 0.05$).

3.6. Cell attachment and viability of hFOB cells on scaffolds

Metabolic cell viability study (Fig. 9) showed no significant variation in cell viability for all scaffold groups during the first two days of culture time, which suggested that the incorporation of PLGA nanoparticles did not affect cell attachment to CH–G porous scaffolds. For all samples,

metabolic cell viability approximately doubled after 5 days cell culture time and then further increased after 11 days culture time. After 5 and 11 days culture time, viability of cells adhered on scaffolds incorporating nanoparticles was only slightly decreased as compared to control samples. However, these differences in cell viability were not significant.

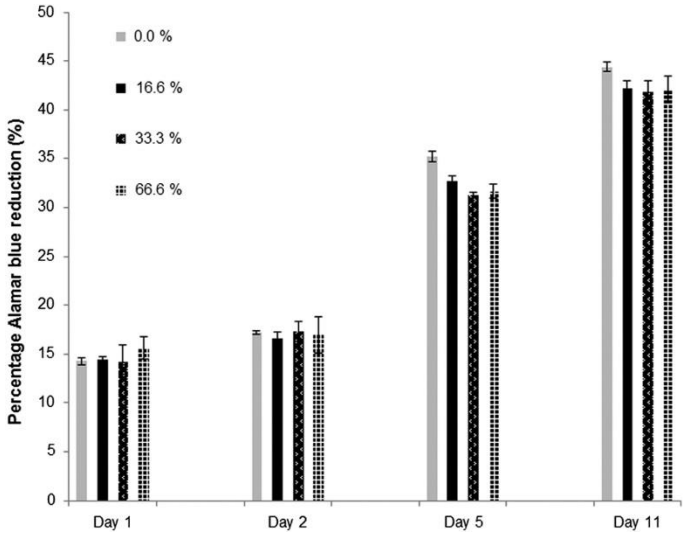

Fig. 9. Effect of PLGA nanoparticle incorporation on metabolic viability (Alamar Blue assay) of hFOB cells seeded onto the scaffolds for 1, 2, 5 and 11 days. Columns are the average data, bars are the standard deviation.

4. Discussion

The choice of the method for biomolecule encapsulation within nanoparticles is usually determined by the solubility characteristics of the drug. In this study, the double emulsion–evaporation process was adopted since it is known to be superior to other incorporation methods in terms of stability of incorporated proteins (Tabata et al., 1993).

The encapsulation efficiency of BSA (used in this study as a model protein) and the particle size were preliminarily optimized by varying the protein:polymer ratio and altering external aqueous phase pH and osmolality. Based on these studies, the maximum encapsulation efficiency was

reached when the amount of polymer was about ten times higher than that of the BSA protein (data not shown). The diffusion of BSA from nanoparticle core toward the aqueous external phase was prevented by properly selecting the pH of external aqueous phase (near to the i.e.p. of BSA) and by increasing its osmolality by adding sodium chloride (data not shown) (Muthu, 2009).

During freezing of CH–G solutions containing PLGA nanoparticles (0.00%–66.6% (w/w)), the interaction of water molecules with the hydrophobic surface of PLGA nanoparticles affected the final pore size distribution of scaffolds. Water molecules in contact with the hydrophobic surfaces of PLGA nanoparticles could not form inter-molecular hydrogen bonds with the hydrophobic surface. Instead, they formed highly connected self-assembled structures by intra-molecular hydrogen bonding with other water molecules. However, an amount of PLGA nanoparticles of 16.6% (w/w) and 33.3% (w/w) only slightly influenced scaffold morphology. On the other hand, CH–G scaffolds loaded with 66.6% (w/w) PLGA nanoparticles showed an increased porosity degree and pore size (75% of pores were larger than 150 μm). This behavior was a consequence of the distribution of nanoparticles within the scaffolds: the PLGA nanoparticles were homogeneously distributed into the scaffold pore walls when they were present at an amount of 16.6%–33.3% (w/w) (Fig. 2(a)–(b)). On the other hand, PLGA nanoparticles formed some aggregates when loaded at 66.6% (w/w) concentration (Fig. 2(c)). A similar result was found by Banerjee et al. for PLGA particles embedded within porous gelatin scaffolds (Banerjee et al., 2009). In addition, the viscosity of the CH–G solution was expected to increase due to PLGA nanoparticle addition in a dose dependent manner (Gong et al., 2006), retarding the water molecule diffusion during freezing and leading to an irregular porous structure as shown in Fig. 5.

Both the hydration degree and the degradation behavior are the most important properties of materials aimed at biomedical or environmental applications, as their lifetime is mainly governed by these two intimately correlated processes. For degradable polymers, degradation occurs as a

result of natural biological processes or other factors such as hydrolysis. Additionally, the drug release rate is mostly influenced by two factors: the diffusion of the drug out of the scaffold and the water uptake of the polymeric matrix. Therefore, the preparation of systems for controlled drug release applications requires the knowledge of water uptake and degradation rate.

In the case of in vitro dissolution tests, scaffolds displayed a similar dissolution degree for PLGA nanoparticle loading in the 0%–33.3% (w/w) range. A significant increase of the dissolution degree was found for the CH–G scaffold loaded with 66.6% (w/w) PLGA nanoparticles: this behavior was probably a consequence of its superior porosity degree and pore size. Furthermore, the time dependent degradation of PLGA particles themselves by means of hydrolysis could have augmented the weight loss percentage in scaffolds with the highest amount of PLGA nanoparticles. The swelling degree of CH–G scaffolds was strongly decreased by the addition of a relatively low amount of PLGA nanoparticles (Fig. 6). Scaffolds with 16.6% (w/w) and 33.3% (w/w) PLGA nanoparticles showed a similar swelling degree; on the other hand, the loading of 66.6% (w/w) PLGA nanoparticles further decreased the swelling degree, probably as a consequence of increased porosity degree and mean pore size.

The incorporation of PLGA nanoparticles within CH–G scaffolds increased the compressive modulus of scaffolds (Fig. 7) in comparison to the control CH–G scaffolds. The compressive modulus increased with increasing PLGA nanoparticles amount from 0% w/w to 33.3% w/w. On the other hand, the compressive modulus of scaffolds containing 66.6% (w/w) PLGA nanoparticles decreased as compared to that of scaffolds containing 33.3% w/w PLGA nanoparticles, probably because of their increased porosity degree and mean pore size. In general, the resistance area of a material sample decreases with increasing pore size and porosity degree, reducing its mechanical resistance. Cell viability studies were performed to examine the effect of the incorporation of hydrophobic nanoparticles within the hydrophilic CH–G scaffolds on cell attachment and cell

viability. Results after 1 *d* and 2 *d* incubation time showed that all scaffolds induced a similar degree of cell attachment (Fig. 9) which indicates that incorporation of PLGA nanoparticles into CH–G scaffolds did not affect cell attachment behavior. However, for scaffolds loaded with different amounts of PLGA nanoparticles, a slight, not significant decrease in cell viability was detected after 5 *d* and 11 *d* culture time. This behavior could be explained by the degradation phenomena involving PLGA nanoparticles and making the local environment slightly acidic.

5. Conclusion

Three-dimensional porous GP-crosslinked CH–G scaffolds incorporated with PLGA nanoparticles were produced as suitable systems for the localized delivery of bioactive agents in scaffolds for bone regeneration, such as growth factors, drugs, etc. This study disclosed the changes in physical properties of porous CH–G scaffolds as a consequence of incorporation of PLGA nanoparticles in three different percentages. The study revealed that loading of hydrophobic PLGA nanoparticles in relatively hydrophilic GP-crosslinked CH–G scaffold altered the scaffold microenvironment and modulated water uptake, compressive modulus, and dissolution properties. On the other hand, incorporation of PLGA nanoparticles within CH–G scaffolds did not affect significantly cell attachment and viability after 1–11 days cell culture time. This study was aimed at the design of an optimized matrix for controlled release of biomolecules for bone tissue engineering applications. Based on the results of this study, the incorporation of 33.3% w/w of PLGA nanoparticles within CH–G scaffolds yielded scaffolds with enhanced mechanical properties, retaining other desirable physical and cell attachment properties. Further studies describing the encapsulation and release of therapeutic proteins, such as Bone Morphogenetic Protein (BMP2)/parathyroid hormone (PTH) from the optimized scaffolds formulations are in progress.

Acknowledgments

The authors acknowledge support for this work provided by Italian Ministry for Research and the University (MIUR) for Vijay Kumar Nandagiri's grant. The authors also acknowledge the assistance by Clara Mattu (Industrial Bio engineering group, Department of Mechanics, Politecnico di Torino) for SEM analysis as well as by Dr. Jacqueline Daly, Dr. John Gleeson and Ms. Ciara Murphy (Department of Anatomy, Bone and Tissue engineering group, Royal College of surgeons in Ireland, Dublin 2, Ireland) for their support in cell studies.

References

Al-Munajjed, A.A., O'Brien, F.J., 2009. Influence of a novel calcium-phosphate coating on the mechanical properties of highly porous collagen scaffolds for bone repair. J. Mech. Beh. Biomed. Mater. 2, 138–146.

Banerjee, I., Mishra, D., Maiti, T.K., 2009. PLGA microspheres incorporated gelatin scaffold: microspheres modulate scaffold properties. Int. J. Biomater. doi:10.1155/2009/143659. Article ID 143659.

Bonadio, J., Smiley, E., Patil, P., Goldstein, S., 1999. Localized, direct plasmid gene delivery in vivo: prolonged therapy results in reproducible tissue regeneration. Nature Med. 5, 753–759.

Borenstein, J.T., Weinberg, E.J., Orrick, B.K., Sundback, C., Kaazempur-Mofrad, M.R., Vacanti, J.P., 2007. Microfabrication of three-dimensional engineered scaffolds. Tissue Eng. 13, 1837–1844.

Chang, C.H., Liu, H.C., Lin, C.C., Chou, C.H., Lin, F.H., 2003. Gelatin–chondroitin–hyaluronan tri-copolymer scaffold for cartilage tissue engineering. Biomaterials 24, 4853–4858.

516 Chiono, V., Pulieri, E., Vozzi, G., Ciardelli, G., Ahluwalia, A., Giusti, P., 2008. Genipin-
517 crosslinked chitosan/gelatin blends for biomedical applications. J. Mater. Sci. Mater. Med. 19, 889–
518 898.
519 Cohen-Sela, E., Chorny, M., Koroukhov, N., Danenberg, H.D., Golomb, G., 2009. A new double
520 emulsion solvent diffusion technique for encapsulating hydrophilic molecules in PLGA
521 nanoparticles. J. Contr. Rel. 33, 90–95.
522 Esposito, E., Cortesi, R., Nastruzzi, C., 1996. Gelatin microspheres: influence of preparation
523 parameters and thermal treatment on chemico-physical and biopharmaceutical properties.
524 Biomaterials 17, 2009–2020.
525 Gong, Y.H., Ma, Z.W., Gao, C.Y., Wang, W., Shen, J.C., 2006. Specially elaborated thermally
526 induced phase separation to fabricate poly(l-lactic acid) scaffolds with ultra large pores and good
527 interconnectivity. J. Appl. Polym. Sci. 101, 3336–3342.
528 Harris, S.A., Enger, R.J., Riggs, B.L., Spelsberg, T.C., 1995. Development and characterization
529 of a conditionally immortalized fetal osteoblastic cell line. J. Bone. Miner. Res. 10, 178–186.
530 Holzer, M., Vogel, V., Mantele, W., Schwartz, D., Haase, W., Langer, K., 2009. Physico-
531 chemical characterization of PLGA nanoparticles after freeze-drying and storage. Eur. J. Pharm.
532 Biopharm. 72, 428–437.
533 Huang, Y., Onyeri, S., Siewe, M., Moshfeghian, A., Madihally, S.V., 2005. In vitro
534 characterization of chitosan–gelatin scaffolds for tissue engineering. Biomaterials 26, 7616–7627.
535 Ito, A., Mase, A., Takizawa, Y., Shinkai, M., Honda, H., Hata, K.I., Ueda, M., Kobayashi, T.,
536 2003. Transglutaminase-mediated gelatin matrices incorporating cell adhesion factors as a
537 biomaterial for tissue engineering. J. Biosci. Bioeng. 95, 196–199.
538 Jeong, B., Bae, Y.H., Lee, D.S., Kim, S.W., 1997. Biodegradable block copolymers as injectable
539 drug-delivery systems. Nature 388, 860–862.

Kawai, K., Suzuki, S., Tabata, Y., Ikada, Y., Nishimura, Y., 2000. Accelerated tissue regeneration through incorporation of basic fibroblast growth factor-impregnated gelatin microspheres into artificial dermis. Biomaterials 21, 489–499.

Keogh, M.B., O'Brien, F.J., Daly, J.S., 2010. A novel collagen scaffold supports human osteogenesis-applications for bone tissue engineering. Cell Tissue Res. 340, 169–177.

Khil, M.S., Cha, D.I., Kim, H.Y., Kim, I.S., Bhattarai, N., 2003. Electrospun nanofibrous polyurethane membrane as wound dressing. J. Biomed. Mater. Res. B Appl. Biomater. 67 (2), 675–679.

Kim, H., Kim, W., Suh, H., 2003. Sustained release of ascorbate-2-phosphate and dexamethasone from porous PLGA scaffolds for bone tissue engineering. Biomaterials 24, 4671–4679.

Kobsa, S., Saltzman, M., 2008. Bioengineering approaches to controlled protein delivery. Pediatr. Res. 63, 513–519.

Lahiji, A., Sohrabi, A., Hungerford, D.S., Frondoza, C.G., 2000. Chitosan supports the expression of extra-cellular matrix proteins in human osteoblasts and chondrocytes. J. Biomed. Mater. Res. 51, 586–595.

Langer, R., 1998. Drug delivery and targeting. Nature 392, 5–10.

Lee, J.E., Kim, K.E., Kwon, I.C., Ahn, H.J., Lee, S.H., Cho, H., Kim, H.J., Seong, S.C., Lee, M.C., 2004. Effects of the controlled–released TGF-beta 1 from chitosan microspheres on chondrocytes cultured in a collagen/chitosan/glycosaminoglycan scaffold. Biomaterials 25 (18), 4163–4173.

Lee, S.H., Shin, H., 2007. Matrices and scaffolds for delivery of bioactive molecules in bone and cartilage tissue engineering. Adv. Drug. Deliv. Rev. 59, 339–359.

563 Ma, P.X., 2008. Biomimetic materials for tissue engineering. Adv. Drug. Deliv. Rev. 60, 184–
564 198.
565 Madihally, S.V., Matthew, H.W.T., 1999. Porous chitosan scaffolds for tissue engineering.
566 Biomaterials 20, 1133–1142.
567 Mi, F.L., 2005. Synthesis and characterization of a novel chitosan–gelatin bioconjugate with
568 fluorescence emission. Biomacromolecules 6, 975–987.
569 Muthu, M.S., 2009. Nanoparticles based on PLGA and its copolymer: an overview. Asian. J.
570 Pharm. 3, 266–273.
571 O'Brien, F.J., Harley, B.A., Yannas, I.V., Gibson, L.J., 2004. Influence of freezing rate on pore
572 structure in freeze-dried collagen-GAG scaffolds. Biomaterials 25, 1077–1086.
573 Perets, A., Baruch, Y., Weisbuch, F., Shoshany, G., Neufeld, G., Cohen, S., 2003. Enhancing the
574 vascularization of three-dimensional porous alginate scaffolds by incorporating controlled release
575 basic fibroblast growth factor microspheres. J. Biomed. Mater. Res. A 65 (4), 489–497.
576 Shen, F., Cui, Y.L., Yang, L.F., Yao, K.D., Dong, X.H., Jia, W.Y., Shi, H.D., 2000. A study on
577 the formation of porous chitosan/gelatin network scaffold for tissue engineering. Polym. Int. 49,
578 1596–1599.
579 Silvia, G.A., Coutinho, O.P., Duchevne, P., Reis, R.L., 2007. Materials in particulate form for
580 tissue engineering. 2. Application in bone. J. Tiss. Eng. Reg. Med. 1, 97–109.
581 Suh, J.K.F., Matthew, H.W.T., 2000. Application of chitosan-based polysaccharide biomaterials
582 in cartilage tissue engineering: a review. Biomaterials 21, 2589–2598.
583 Tabata, Y., Takebayashi, Y., Ueda, T., Ikada, Y., 1993. A formulation method using D, L-lactic
584 acid oligomer for protein released with reduced initial burst. J. Control. Rel. 23, 55–64.

585 Tachibana, A., Nishikawa, Y., Nishino, M., Kaneko, S., Tanabe, T., Yamauchi, K., 2006.
586 Modified keratin sponge: binding of bone morphogenetic protein-2 and osteoblast differentiation.
587 J. Biosci. Bioeng 102, 425–429.
588 Thein-Han, W.W., Saikhun, J., Pholpramoo, C., Misra, R.D.K., Kitiyanant, Y., 2009. Chitosan–
589 gelatin scaffolds for tissue engineering: physico-chemical properties and biological response of
590 buffalo embryonic stem cells and transfectant of GFP–buffalo embryonic stem cells. Acta
591 Biomater. 5, 3453–3466.
592 VandeVord, P.J., Matthew, H.W., DeSilva, S.P., Mayton, L., Wu, B., Wooley, P.H., 2002.
593 Evaluation of the biocompatibility of a chitosan scaffold in mice. J. Biomed. Mater. Res. 59, 585–
594 590.
595 Vasita, R., Katti, D.S., 2006. Growth factor-delivery systems for tissue engineering: a materials
596 perspective. Expert. Rev. Med. Dev. 3, 29–47.
597 Zhao, F., Yin, Y., Lu, W.W., Leong, J.C., Zhang, W., Zhang, J., Zhang, M., Yao, K., 2002.
598 Preparation and histological evaluation of biomimetic three-dimensional hydroxyapatite/chitosan–
599 gelatin network composite scaffolds. Biomaterials 23, 3227–3234.
600 Zisch, A.H., Lutolf, M.P., Hubbell, J.A., 2003. Biopolymeric delivery matrices for angiogenic
601 growth factors. Cardiovasc. Pathol. 12, 295–310.